SUPPLEMENTARY INFORMATION

Electrolyte Modulators towards Polarization Immune Lithium-Ion Batteries for Sustainable Electric Transportation

Xinru Li[1], Pengcheng Xu[1], Yue Tian[2], Alexis Fortini[1], Seung Ho Choi[1], Xiaoyan Liu[2], Jinhui Xu[1], Qian Liu[3], Hao Bin Wu[3], Gen Chen[1], Chen Zhang[1], Xinyi Tan[1], Lihua Jin[4], Qinchao Wang[5], Li Shen[1,*] and Yunfeng Lu[1,*]

[1]Department of Chemical and Biomolecular Engineering, University of California, Los Angeles, 420 Westwood Plaza, Los Angeles, California, 90095, United States.

[2]Education Ministry Key Lab of Resource Chemistry and Shanghai Key Laboratory of Rare Earth Functional Materials, Department of Chemistry, Shanghai Normal University, Shanghai 200234, P. R. China.

[3]School of Materials Science and Engineering, Zhejiang University, Hangzhou 310027, P. R. China.

[4]Department of Mechanical and Aerospace Engineering, University of California, Los Angeles, 420 Westwood Plaza, Los Angeles, California, 90095, United States.

[5]Chemistry Division, Brookhaven National Laboratory, Upton, NY 11973, United States.

*Corresponding author. Email: lishen@ucla.edu, luucla@ucla.edu

1. Material Characterization

The crystal structure of UMCM-309a was characterized by x-ray diffraction with a Rigaku powder X-ray diffractometer (XRD) using Kα radiation (λ = 1.54 Å). The morphology was observed by field scanning electron microscopy (Nova 230 Nano SEM) and transmission electron microscopy (FEI T12 Quick CryoEM and CryoET TEM). N_2 adsorption/desorption measurements were conducted by using a Micromeritics ASAP 2020 system at 77 K. Prior to

the measurement, a pristine UMCM-309a sample was degassed at 180 °C for 12 h. The Brunauer-Emmett-Teller (BET) method was employed to determine the specific surface area, and the Density functional theory (DFT) model was applied to calculate pore diameter. The morphology of a UMCM-309a nanosheet was characterized by atomic force microscopy (AFM) (AFM5200S; Hitachi High-Technologies Corporation). The sample was prepared by exfoliating the nanosheets, which were deposited on Si wafers. The Young's modulus of the electrolyte interface was measured by a scanning probe microscope (SPM-9700HT, Shimadzu Corp) using a silicon tip OMCL-AC240TS (resonance frequency = 70 kHz and force constant =2 N m^{-1}). ^{19}F NMR and ^{7}Li NMR spectra were obtained from a Bruker DMX500 (500 MHz) spectrometer. All ^{19}F NMR and ^{7}Li NMR samples were prepared by completely digesting 50 µL LFS with 0.2 wt.% MEM and LFS samples in 500 µL of deuterium oxide (D_2O). XAS was performed at beamline 7-BM of the National Synchrotron Light Source II at Brookhaven National Laboratory. Zr K-edge XAS spectra were collected in transmission mode. The XAS data were processed using Athena and Artemis software packages. Inductively coupled plasma (ICP) optical emission spectroscopy was conducted using a Shimadzu ICP-9000. Thermogravimetric analysis (TGA) was carried out in argon atmosphere by a ramping rate of 10 °C min^{-1}. Raman spectroscopy was conducted on a Renishaw 2000 System with a He/Ne laser at a wavelength of 633 nm. The zeta potential was measured using a Malvern Zetasizer ZS. X-ray photoelectron spectroscopy (XPS) measurements were performed on an AXIS Ultra DLD instrument. The samples were prepared in a glovebox before quickly being transferred to a high-vacuum chamber.

2. Supplementary Figures and Tables

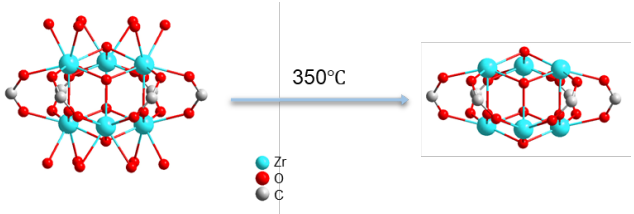

Supplementary Figure 1. Schematic illustration of thermal activation process of UMCM-309a that generates OMSs.

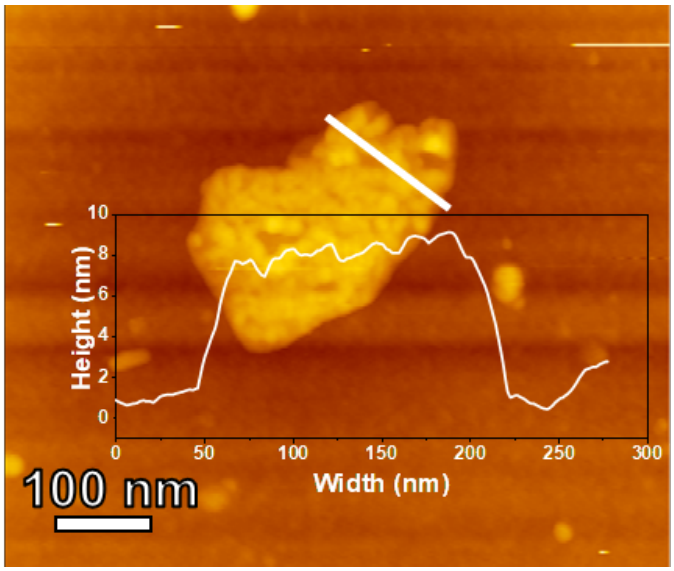

Supplementary Figure 2. AFM micrograph and height distribution of UMCM-309a measured along the white line.

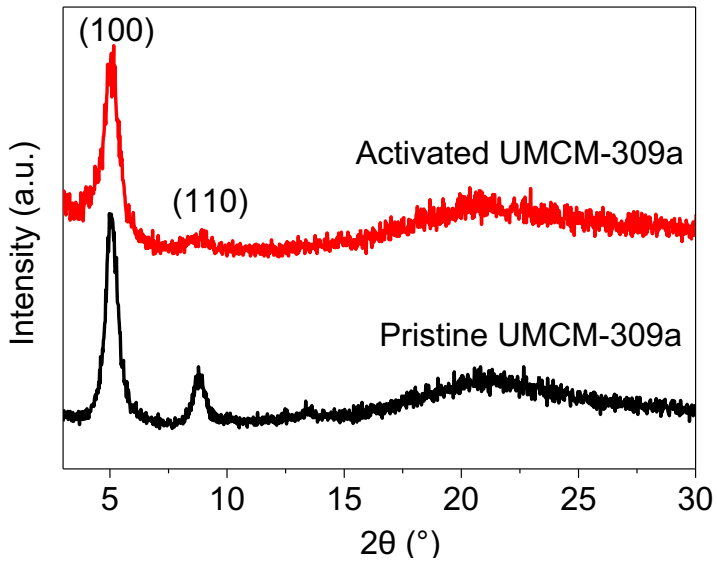

Supplementary Figure 3. PXRD patterns of pristine UMCM-309a and activated UMCM-309a.

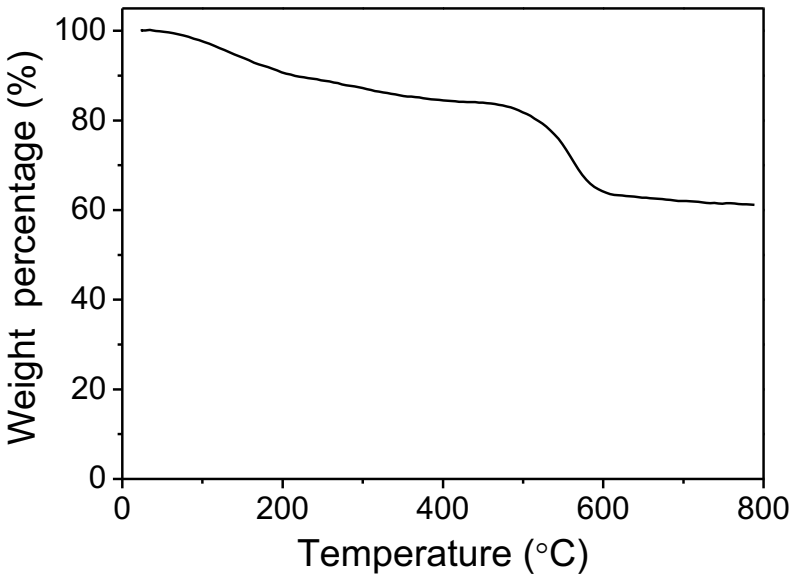

Supplementary Figure 4. Thermogravimetric analysis (TGA) curve of pristine UMCM-309a in argon flow. The TGA curve displays two segments of weight loss. The first gradual loss (~15%) up to 400 ℃ is ascribed to the elimination of guest molecules and capping hydroxyl groups.[1] The subsequent second loss (~ 25%) arises from the decomposition of the organic linkers (BTB) or structural collapse, supporting superior thermal stability of UMCM-309a. Thus, an activation temperature of 350 ℃ was used in this work.

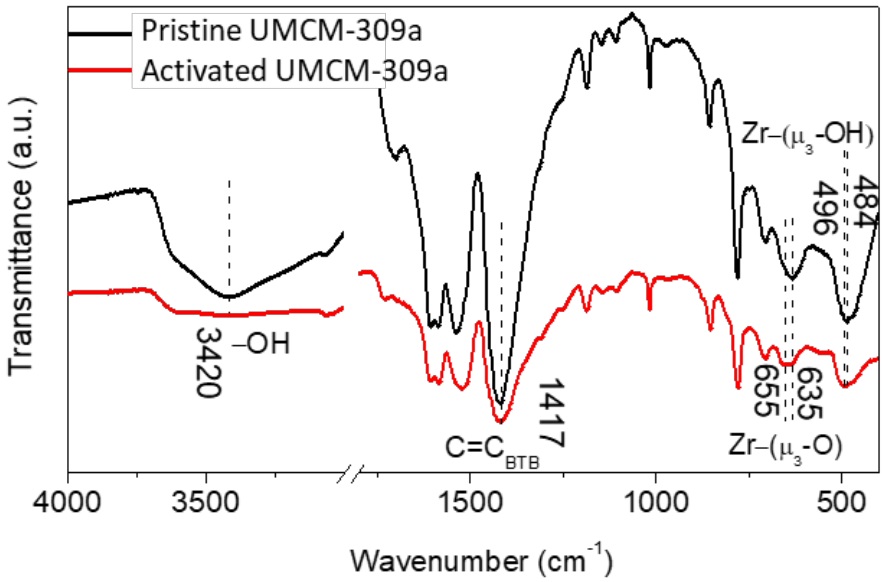

Supplementary Figure 5. IR spectra of pristine UMCM-309a and activated UMCM-309a.

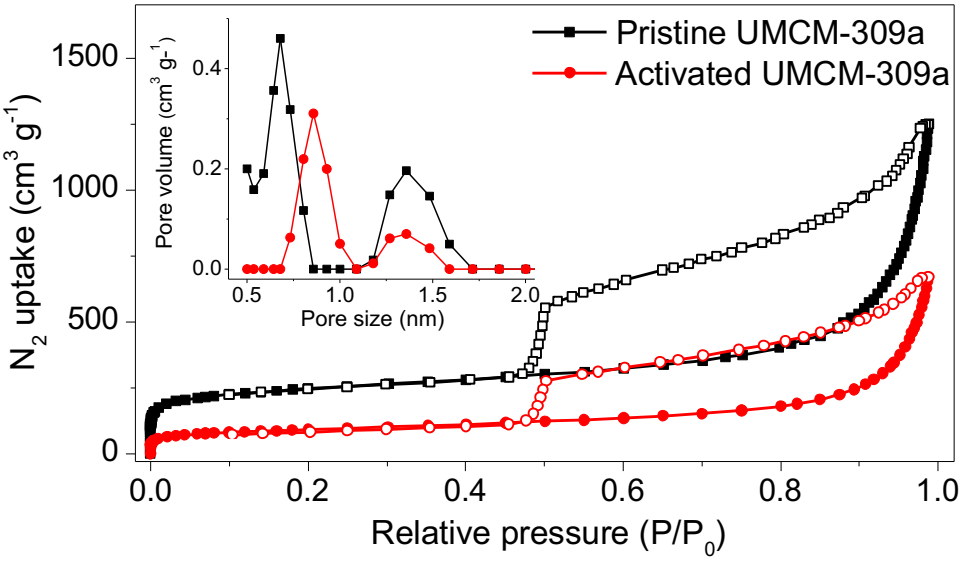

Supplementary Figure 6. N_2 adsorption isotherms of pristine and activated UMCM-309a measured at 77 K. Inset shows the pore size distributions calculated using DFT slit-pore model. Compared with the pristine sample, the activated UMCM-309a exhibits decreased surface area/pore volume (315 m^2 g^{-1}/0.5 cm^3 g^{-1} vs 831 m^2 g^{-1} and 0.9 cm^3 g^{-1}), in addition to increased micropore size (8.6/13.7 Å vs 6.8/13.6 Å), which originates from shrinkage of the nanosheets and expanded interlayer spacing due to removal of the hydroxyl groups, respectively.[2]

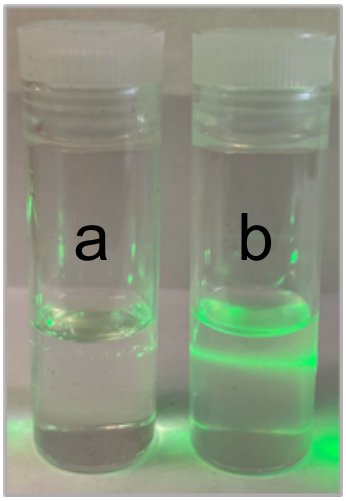

Supplementary Figure 7. A photograph showing Tyndall effect in solutions with different compositions: (a) LFS and (b) LFS with MEM.

Supplementary Table 1. Summary of mass and molar concentration of Zr/Li by ICP-AES analysis of LFS-laden MEM.

Element	Mass concentration (mg kg^{-1})	Molar concentration (mmol kg^{-1})
Zr	115.4899	1.2691
Li	43.6985	6.2426

Supplementary Note 1. Enrichment of LiTFSI in MEM

To assess the molar concentration of LiTFSI in LFS-laden MEM, the volume of solvent (DOL/DME) was determined by drying 1 g LFS-laden MEM particles at 100 °C for 3 days (under vacuum). The weight loss (0.48 g) corresponds to 0.5 mL of the solvent (0.48 g / 0.95 g mL^{-1}).[3] According to the ICP result, the mole ratio between Li and Zr is ~ 4.92 (Li/Zr = 4.92), suggesting the molar ratio of LiTFSI *vs* MEM unit ($Zr_6(\mu_3\text{-}O)_4(\mu_3\text{-}OH)_4(BTB)_2$) is 29.52. If the dried sample contains x grams of LiTFSI, the mass of MEM will be (0.52 – x) g.

$$(x \text{ g} / 287 \text{ g mol}^{-1}) / ((0.52 - x) \text{ g} / 1554 \text{ g mol}^{-1}) = 29.52$$

The resulting mass and moles of the LiTFSI are calculated to be 0.44 g and 1.53 mmol, respectively. Hence, the molar concentration of LiTFSI is around 3.06 M (1.53 mmol / 0.5 mL) in MEM.

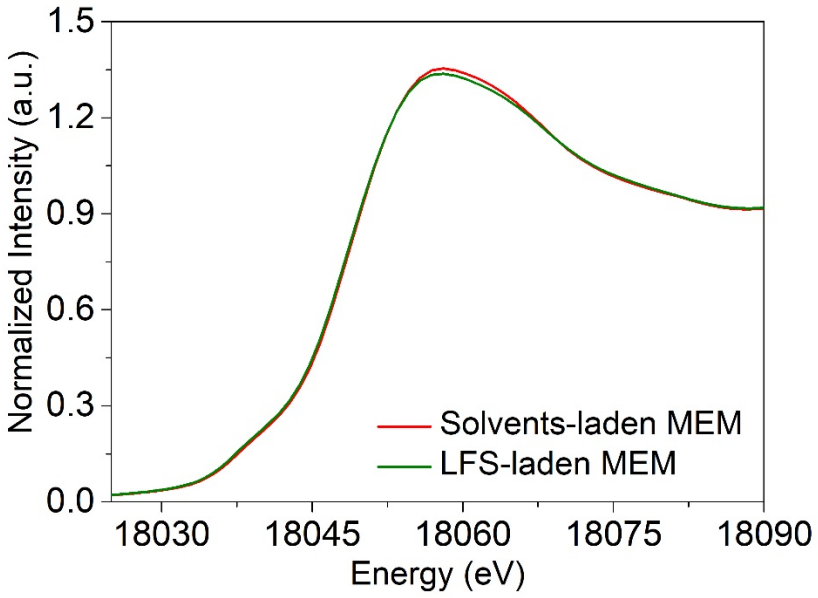

Supplementary Figure 8. Zr K-edge EXAFS spectra in R-space for solvent-laden MEM and LFS-laden MEM.

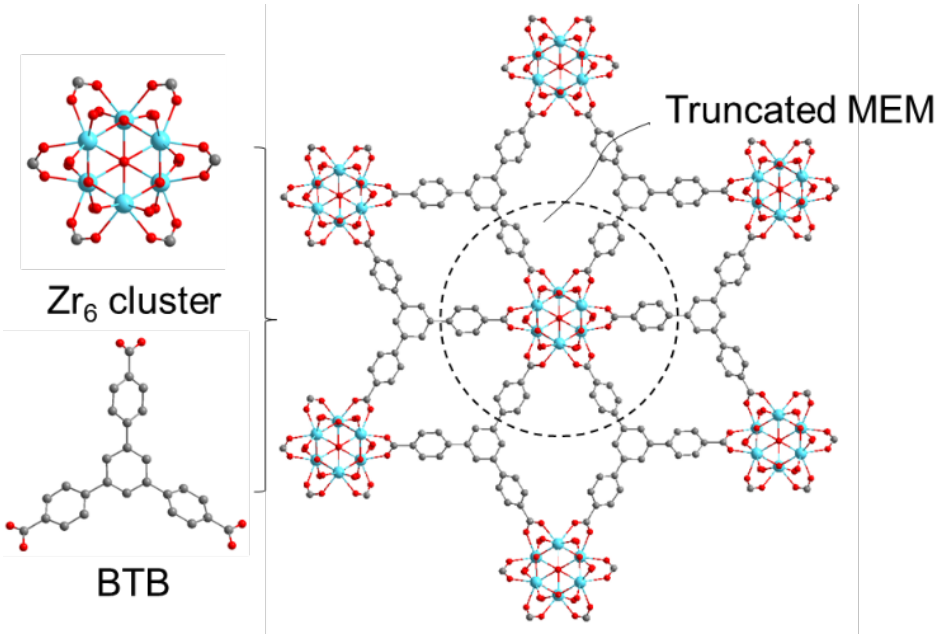

Supplementary Figure 9. Truncated MEM for DFT study (cyan: Zr, red: O, grey: C).

Supplementary Table 2. DFT calculations of $TFSI^-$ adsorption configurations at different initial positions on MEM clusters

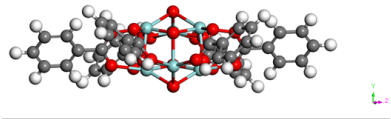 MEM cluster	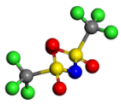 $TFSI^-$
E = -96591.050 eV	E = -49677.469 eV
C, O, Zr, F, N, S, H	

Initial position	Geometry optimization
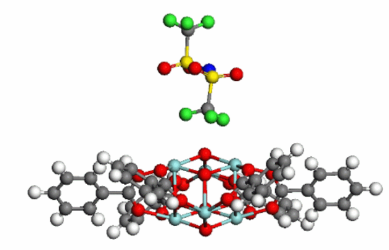	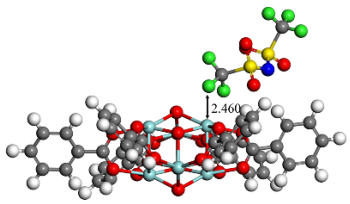
E_{link1} = -146272.008 eV	E_{ads1} = -3.489 eV
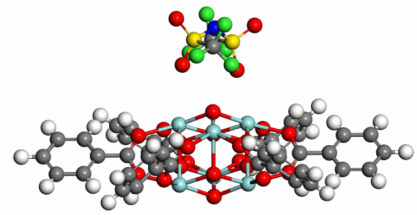	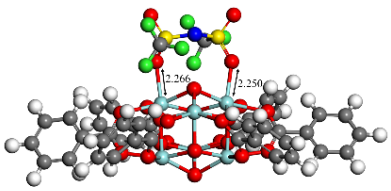
E_{link2} = -146273.819 eV	E_{ads2} = -5.300 eV
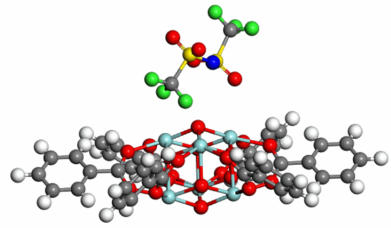	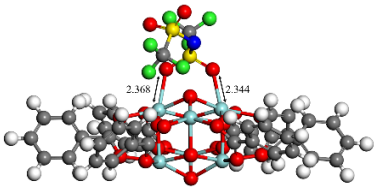
E_{link3} = -146273.644 eV	E_{ads3} = -5.126 eV

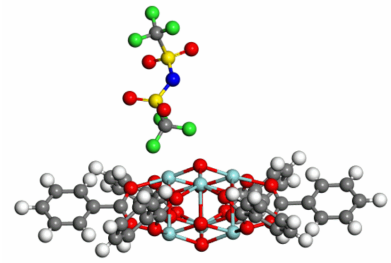	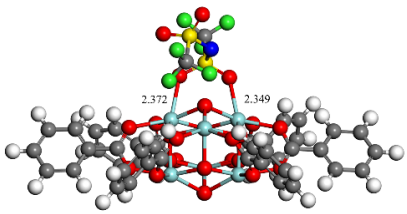
E_{link4} = -146273.690 eV	E_{ads4} = -5.171 eV
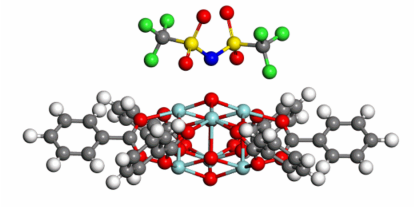	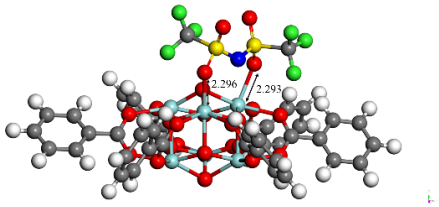
E_{link5} = -146274.040 eV	E_{ads5} = -5.521 eV
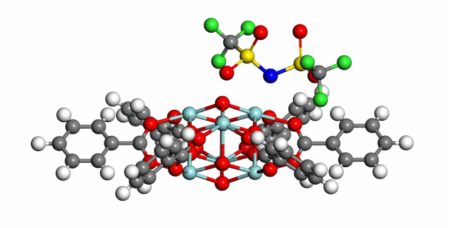	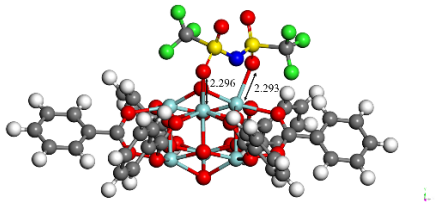
E_{link6} = -146274.054 eV	E_{ads6} = -5.535 eV
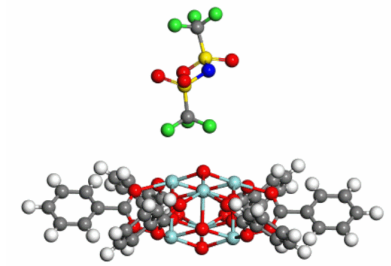	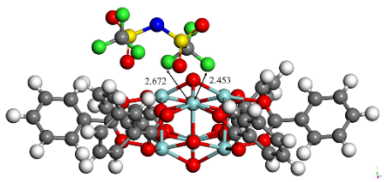
E_{link7} = -146272.037 eV	E_{ads7} = -3.518 eV
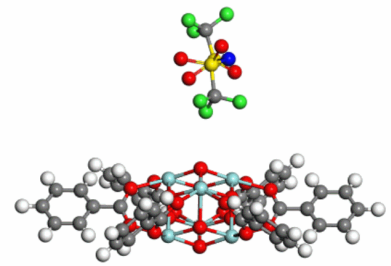	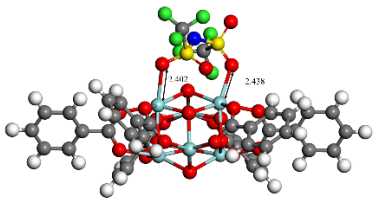
E_{link8} = -146273.986 eV	E_{ads8} = -5.467 eV

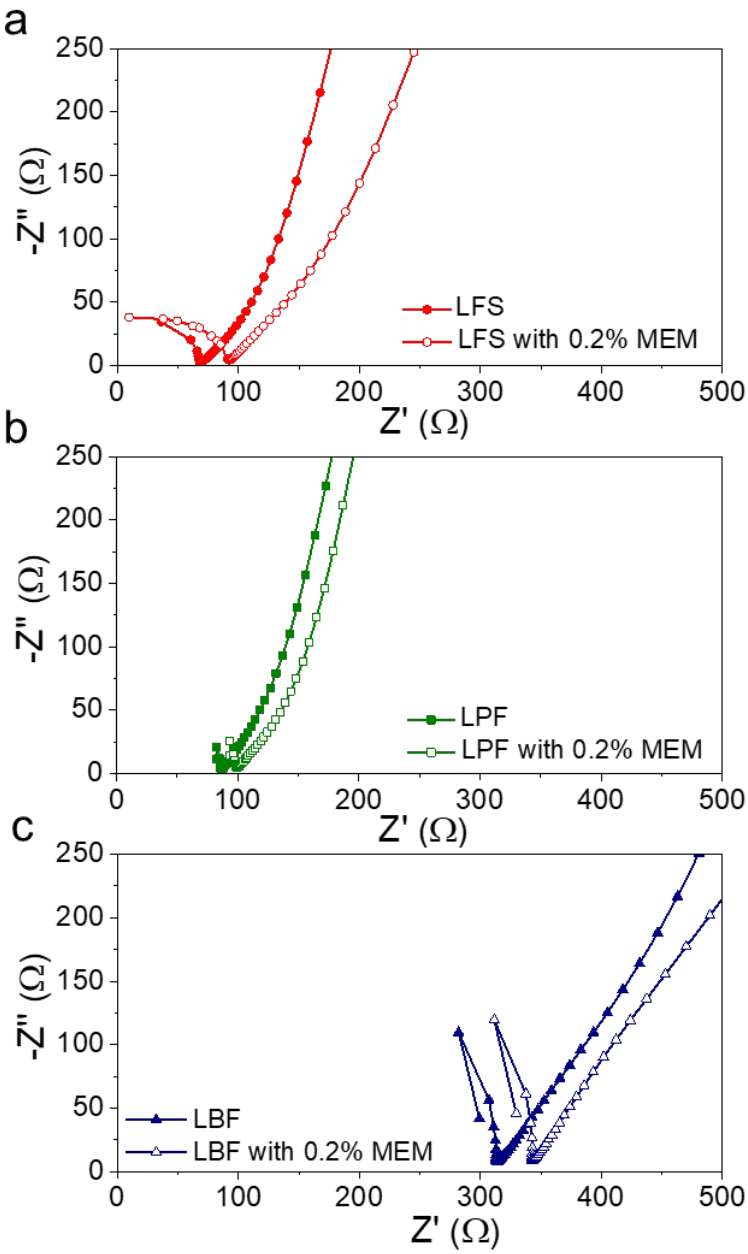

Supplementary Figure 10. Nyquist plots for measuring the ionic conductivity of electrolytes: (a) LFS and LFS with 0.2 wt.% MEM; (b) LPF and LPF with 0.2 wt.% MEM; (c) LBF and LBF with 0.2 wt.% MEM. The ionic resistance was estimated by the extrapolated interception of the Nyquist plots with real axis.

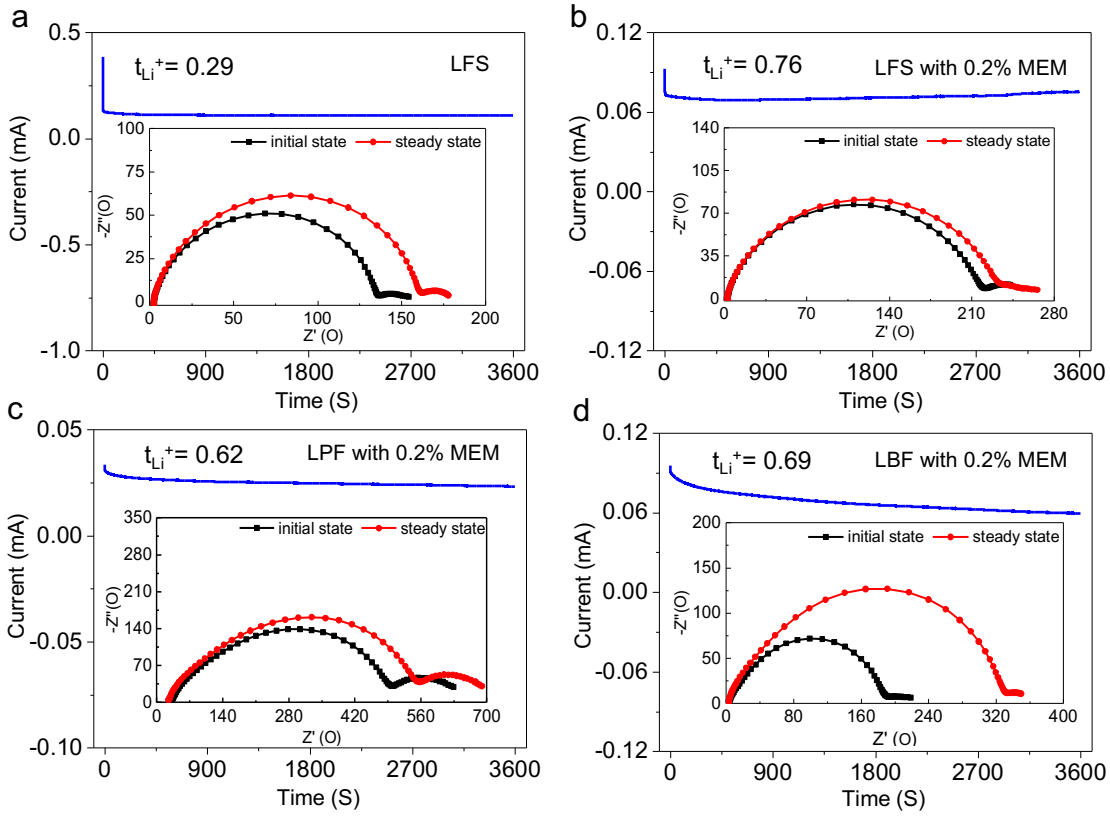

Supplementary Figure 11. Potentiostatic polarization of electrolytes in Li|Li cells (inset: Nyquist plots of initial and steady states). (a) LFS; (b) LFS with 0.2 wt.% MEM; (c) LPF with 0.2 wt.% MEM; (d) LBF with 0.2 wt.% MEM.

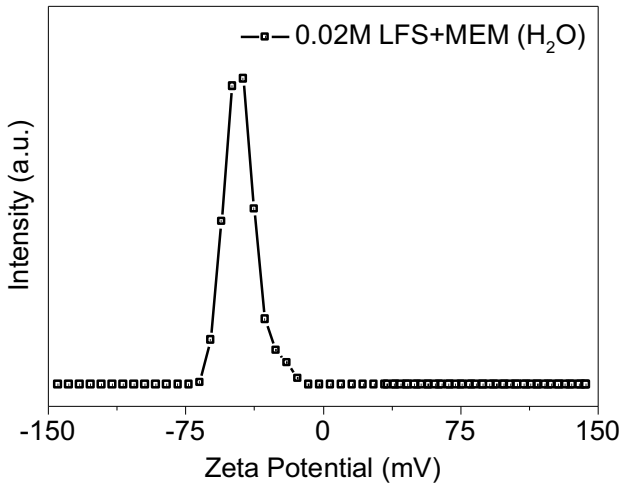

Supplementary Figure 12. Zeta potential of 0.2 wt.% MEM in 0.02 M LiTFSI aqueous solution.

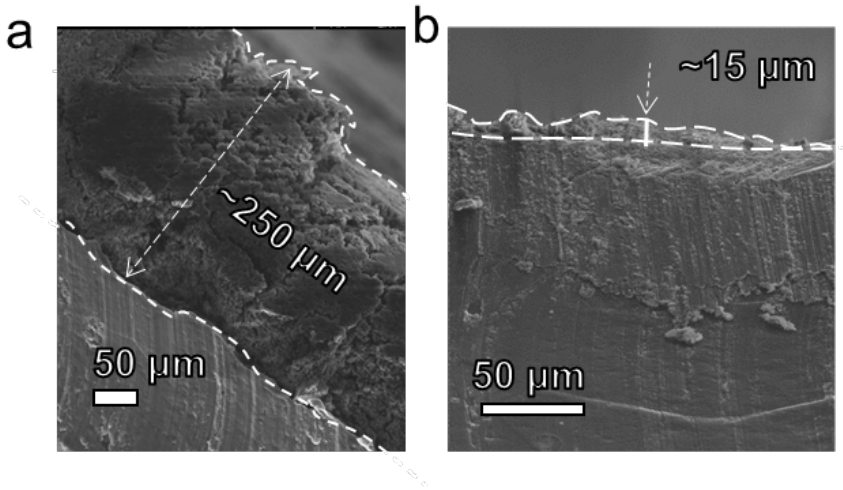

Supplementary Figure 13. SEM images of the cross-section view of the lithium foil: (a) LFS; (b) LFS with 0.2 wt.% MEM.

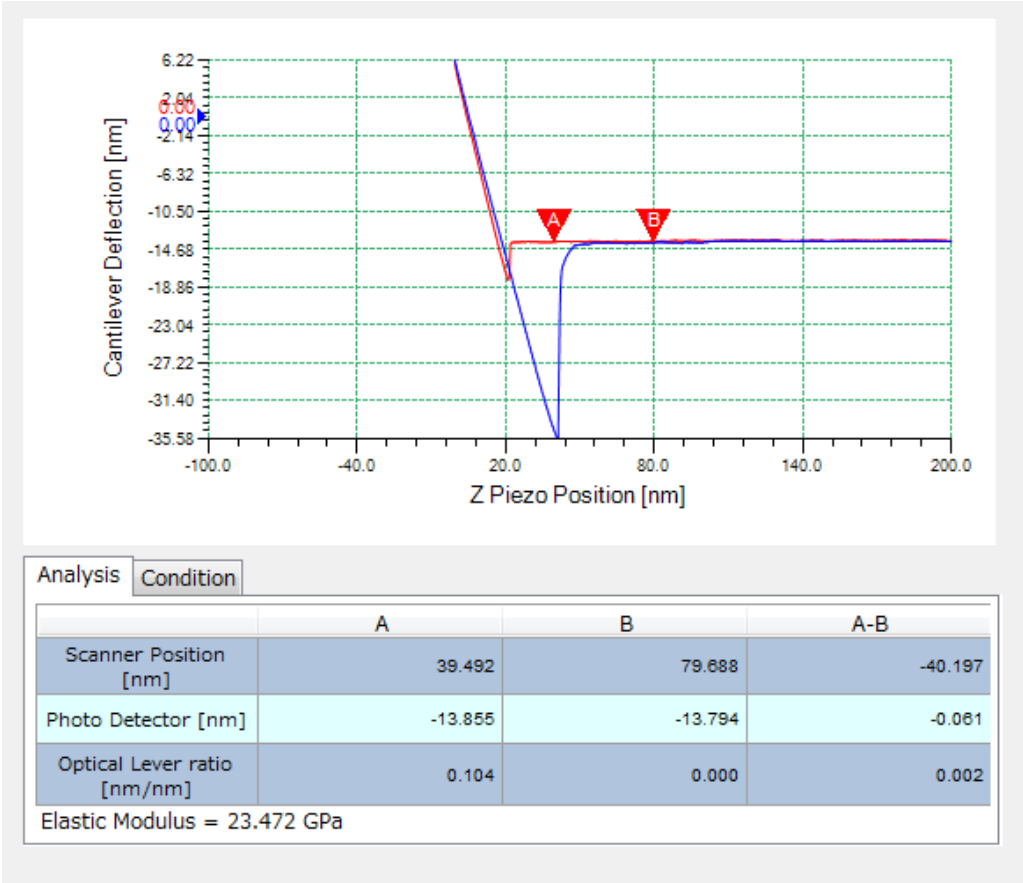

Supplementary Figure 14. Measurement of the elastic modulus (AFM) for cycled Li using LFS with 0.2 wt.% MEM.

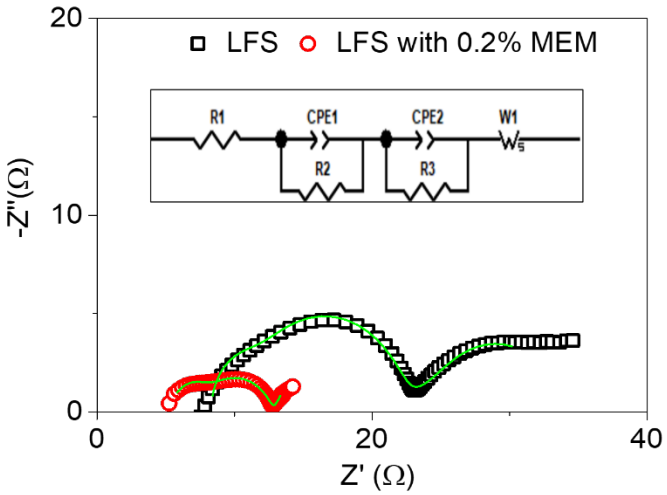

Supplementary Figure 15. Nyquist plots of the cycled Li|Li cells with LFS and LFS with 0.2 wt.% MEM (25th cycles), where the inset shows an equivalent circuit, and the green curves represent corresponding fitting results. Notes: (1) the sum of R2 and R3 is denoted as interfacial resistance in Li|Li cell, which could be estimated from the semicircle diameters; (2) R1 denotes the ohmic resistance, which could be estimated from the first plot interception with real axis at high frequency.

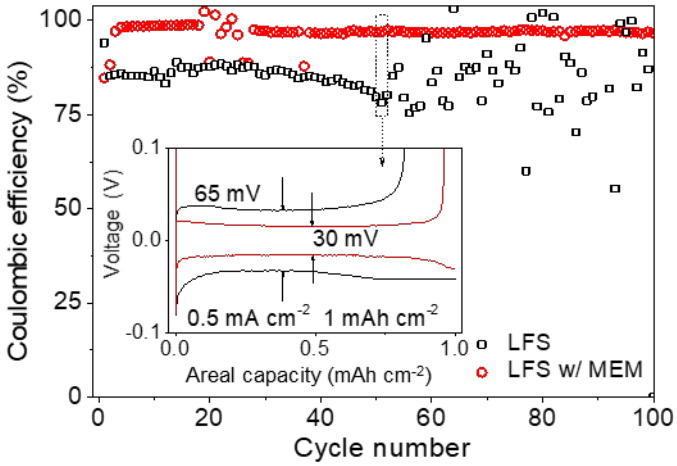

Supplementary Figure 16. Coulombic efficiency of Cu|Li cells cycled at a plating areal capacity of 1 mAh cm^{-2} (inset: voltage profiles at 50th cycle).

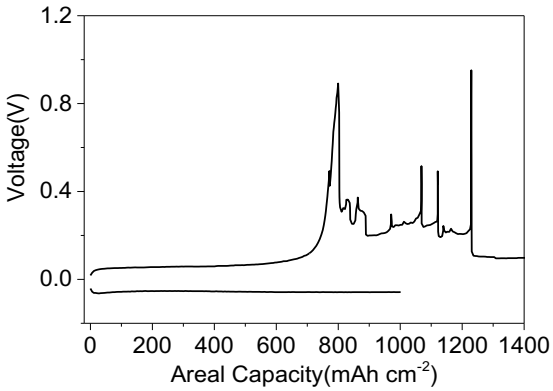

Supplementary Figure 17. The voltage-capacity plot of a Cu|Li cell using LFS at the 99th cycle. Note: the zigzag shape of charging curves indicates proliferation of dendritic Li.

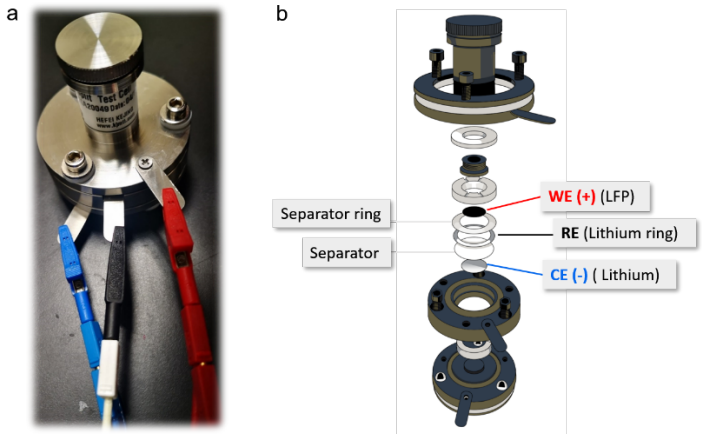

Supplementary Figure 18. (a) A photograph and (b) an exploded schematic view of three-electrode flow cell setup**.**

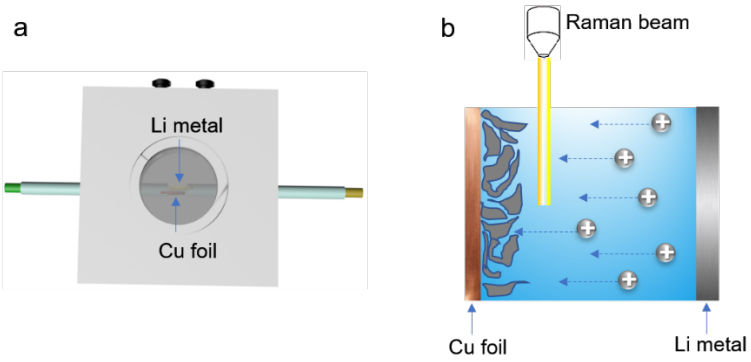

Supplementary Figure 19. Apparatus setup of *in-situ* Raman measurement. (a) Illustration of custom-made Cu|Li cell with a quartz window; (b) Illustration of the Raman beam being focused in the cell.

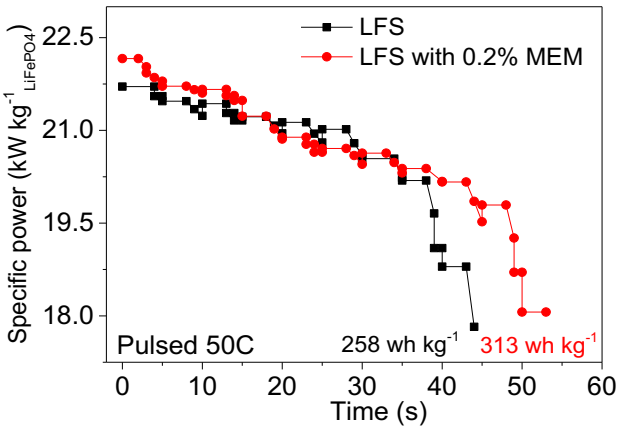

Supplementary Figure 20. Discharge profiles of $LiFePO_4$|Li cells at pulsed discharged at a C-rate of 50, where the reference and modulated cell deliver an energy output of 258 and 313 wh kg^{-1}, respectively.

3. COMSOL Simulations

3.1. Transport Equations (all governing equations are adopted from Batteries & Fuel Cells Module (2018). COMSOL. Retrieved November 24, 2020, from https://doc.comsol.com/5.4/doc/com.comsol.help.bfc/BatteriesAndFuelCellsModuleUsersGuide.pdf)

In order to draw further insights by relating electrolyte parameters to electrochemical performance, simulations were employed to model the cells measured in the lab using COMSOL software. The effect of several key properties on electrochemical performance, including the ionic conductivity (σ_l) and lithium transference (or transport) number (t_{Li^+}), were investigated. There are five dependent variables for this system, the electrolyte potential, ϕ_l [V], the electric potential in the electrodes, ϕ_s [V], the potential losses due to the solid-electrolyte interface (SEI) in the porous electrodes, $\Delta\phi_{s,\mathrm{film}}$ [V], the salt concentration in the electrolyte c_l [mol m^{-3}], and the solid lithium concentration in the electrode particles, c_s [mol m^{-3}]. For the porous electrode domain, an extra pseudo dimension, r, is used to describe the transport of solid lithium through the active material particles using Fick's law. The c_s variable is solved for in the extra dimension, using an internal discretization in the particle dimension, r [m], not visible in the ordinary model geometry, which allows the

surface, center and average values of c_s to be evaluated in the real dimension, x [m]. The domain equations in the electrolyte are the conservation of current and the mass balance for the salt. The conservation of current is shown in Equation 1, where $\sigma_{l,\text{eff}}$ [S m^{-1}] is the effective electrolyte conductivity, R [J mol^{-1} K^{-1}] is gas constant, T [K] is the temperature, F [C mol^{-1}] is Faraday's constant, f is the activity coefficient for the salt, and i_l [C m^{-2} s^{-1}] is the current at any point in the electrolyte.

$$i_l = -\sigma_{l,\text{eff}} \nabla \phi_l + \frac{2\sigma_{l,\text{eff}} RT}{F} \left(1 + \frac{\partial \ln f}{\partial \ln c_l}\right) (1 - t_{\text{Li}^+}) \nabla c_l \tag{1}$$

The total current density, $i_{v,\text{total}}$ [C m^{-2} s^{-1}], is defined by Equation 2, where Q_l [C m^{-2} s^{-1}] is an arbitrary current source term.

$$i_{v,\text{total}} + Q_l = \nabla \cdot i_l \tag{2}$$

The mass balance for the lithium ions in the electrolyte is shown by Equation 3 and 4, where ε_l is the electrolyte porosity, N_I [mol m^{-2} s^{-1}] is the flux of lithium ions in the electrolyte, $D_{l,\text{eff}}$ [m^2 s^{-1}] is the effective electrolyte salt diffusivity, and R_l [mol s^{-1}] is the lithium-ion source term in the electrolyte.

$$\varepsilon_l \frac{\partial c_l}{\partial t} + \nabla \cdot N_I = R_l \tag{3}$$

$$N_I = -D_{l,\text{eff}} \nabla c_l + \frac{i_l t_{\text{Li}^+}}{F} \tag{4}$$

The source term in the mass balance in Equation 3, R_l [mol m^{-3} s^{-1}], is calculated from Equation 10, where $i_{v,m}$ [C m^{-2} s^{-1}] is the current from the charge transfer reaction, $i_{\text{dl},m}$ [C m^{-2} s^{-1}] is the current from the double layer capacitance, $\nu_{\text{Li}^+,m} = -1$ and $n_m = 1$ for the lithium insertion reaction, and $R_{l,\text{src}}$ [mol m^{-3} s^{-1}] is an additional reaction source that can be added to the existing reaction sources, which is not necessary in this model. Equations 1 through 5 are also used for the electrolyte in the separator, but with $R_l = 0$.

$$R_l = -\sum_m \frac{\nu_{\mathrm{Li}^+,m} i_{v,m}}{n_m F} - \frac{\nu_{\mathrm{Li}^+,m} i_{\mathrm{dl},m}}{n_m F} + R_{l,\mathrm{src}} \tag{5}$$

In the solid electrode particles, the current density, i_s [C m^{-2} s^{-1}], is defined by Equation 6, where σ_s [S m^{-1}] is the effective electrical conductivity.

$$i_s = -\sigma_s \nabla \phi_s \tag{6}$$

The total current density, $i_{v,\mathrm{total}}$ [C m^{-2} s^{-1}], can also be defined by Equation 7, where Q_s [C s^{-1}] is an arbitrary current source term.

$$-i_{v,\mathrm{total}} + Q_s = \nabla \cdot i_s \tag{7}$$

Inside the solid particles, lithium diffuses to and from the surface. The mass balance for solid lithium is shown by Equation 8, where D_s [m^{2}s^{-1}] is the solid-phase diffusivity in the solid electrode particles. This equation is solved locally by the physics interface in a pseudo 1D dimension, with the solid phase concentrations at the nodal points for the element discretization of the particle as the independent variables.

$$\frac{\partial c_s}{\partial t} = \nabla \cdot (D_s \nabla c_s) \tag{8}$$

The electrode reaction, converting solid lithium to and from lithium ions, occurs at the particle surface. Using Butler-Volmer kinetics, the local current, $i_{\mathrm{loc},m}$ [C m^{-2} s^{-1}] is defined by Equation 9, where i_0 [C m^{-2} s^{-1}] is the transfer current at zero overpotential, α_a is the anodic transfer coefficient, α_c is the cathodic transfer coefficient, and η [V] is the overpotential.

$$i_{\mathrm{loc},m} = i_0 \left(\exp\left(\frac{\alpha_a F \eta}{RT}\right) - \exp\left(\frac{\alpha_c F \eta}{RT}\right) \right) \tag{9}$$

The transfer current at zero overpotential, i_0 [C m^{-2} s^{-1}], is defined by Equation 10, where k_a [m s^{-1}] is the anodic rate constant, k_c [m s^{-1}] is the cathodic rate constant, $c_{s,\max}$ [mol m^{-3}] is the maximum solid lithium concentration, and c_{ref} [mol m^{-3}] is the reference concentration.

$$i_0 = F(k_a)^{\alpha_c}(k_c)^{\alpha_a}\left(c_{s,\max} - c_s\right)^{\alpha_a}(c_s)^{\alpha_c}\left(\frac{c_l}{c_{\text{ref}}}\right) \tag{10}$$

The current from the charge transfer reaction $i_{v,m}$ [C $\cdot$ m^{-2} $\cdot$ s^{-1}] is the local current, $i_{\text{loc},m}$ [C m^{-2} s^{-1}], multiplied by the specific surface area of the active material particles in the electrode, $A_{\text{v,m}}$ [m^2 m^{-2}], which is shown by Equation 11.

$$i_{v,m} = A_{\text{v},m} i_{\text{loc},m} \tag{11}$$

The total current density, $i_{v,\text{total}}$ [C m^{-2} s^{-1}], is the sum of the current from all the charge transfer reactions (only one in this model) and the current from the double layer capacitance, $i_{\text{dl},m}$ [C m^{-2} s^{-1}], which is shown by Equation 12. The current from the double layer capacitance is ignored in this model.

$$i_{v,\text{total}} = \sum_m i_{v,m} + i_{\text{dl},m} \tag{12}$$

At the surface of the solid particles, the boundary condition for the flux of lithium is defined by Equation 13, where $\nu_{\text{Li}\Theta,m} = 1$ and $n_m = 1$ for the lithium insertion reaction, and N_{shape} equals 3 for spherical particles.

$$-D_s \left.\frac{\partial c_s}{\partial r}\right|_{r=r_p} = -\sum_m \frac{\nu_{\text{Li}\Theta,m} i_{v,m}}{n_m F} \frac{r_p}{N_{\text{shape}} \varepsilon_s} \tag{13}$$

At the center of the particles, there is a no flux condition, where the change in concentration with respect to r is zero. This boundary condition is shown by Equation 14.

$$\left.\frac{\partial c_s}{\partial r}\right|_{r=0} = 0 \tag{14}$$

To account for the effect of porosity in the diffusivities, the Bruggeman model is used to calculate the effective liquid-phase diffusivity, $D_{l,\text{eff}}$ [$\text{m}^2\,\text{s}^{-1}$], according to Equation 15 and the effective electrolyte conductivity, $\sigma_{l,\text{eff}}$ [$\text{S}\,\text{m}^{-1}$], according to Equation 16, where ε_l is the electrolyte porosity, and β is the Bruggeman coefficient.

$$D_{l,\text{eff}} = D_l \varepsilon_l{}^{\beta} \tag{15}$$

$$\sigma_{l,\text{eff}} = \sigma_l \varepsilon_l \tag{16}$$

The electrochemical reactions in this physics interface are assumed to be insertion reactions occurring at the surface of small solid spherical particles of radius r_p [m], in the electrodes. Since the total concentration of reaction sites, $c_{s,\max}$ [$\text{mol}\,\text{m}^{-3}$], is assumed to be constant, the concentration of the of free reaction sites, c_{Θ_s} [$\text{mol}\,\text{m}^{-3}$], which is defined by Equation 17, does not need to be solved for to obtain ∇c_s or $\frac{\partial c_s}{\partial t}$.

$$c_{\Theta_s} = c_{s,\max} - c_s \tag{17}$$

One important parameter for the insertion of lithium into electrodes, the state-of-charge (SOC) for the solid particles, is defined by Equation 18.

$$\text{SOC} = \frac{c_s}{c_{s,\max}} \tag{18}$$

To model a film resistance from the SEI layer, an extra variable for the potential variation over the film, $\Delta\phi_{s,\text{film}}$ [V], is defined by Equation 19, where R_{film} [Ω] is the generalized film resistance. However, the film resistance is ignored in this model.

$$\Delta\phi_{s,\text{film}} = i_{\text{tot}} R_{\text{film}} \tag{19}$$

The activation overpotential, η [V], for all electrode reactions in the electrode is shown by Equation 20, where E_{eq} [V] is the equilibrium potential, also known as the open-circuit potential, which is given as a function of SOC in the COMSOL $LiFePO_4$ material properties.

$$\eta = \phi_s - \Delta\phi_{s,\text{film}} - \phi_l - E_{\text{eq}} \tag{20}$$

For the lithium metal anode, the same charge-transfer equations are used, except different equations are needed for the overpotential, η [V], and the transfer current at zero overpotential, i_0 [C m^{-2} s^{-1}], since the lithium anode is modeled as an electrode surface instead of a porous electrode. For an electrode surface, the overpotential is shown by Equation 21, where $\phi_{s,\text{ext}} = 0$ is the external potential, and the transfer current at zero overpotential is shown by Equation 22.

$$\eta = \phi_{s,\text{ext}} - \phi_l - E_{\text{eq}} \tag{21}$$

$$i_0 = F(k_a)^{\alpha_c}(k_c)^{\alpha_a}\left(\frac{c_l}{c_{\text{ref}}}\right) \tag{22}$$

A few more boundary conditions and initial values need to be specified to complete the transport equations needed for the LIB model. At the current collector surface next to the porous electrode, there is a zero-flux condition, given by Equation 23, since no lithium ions can move past this boundary.

$$-n \cdot N_I = 0 \tag{23}$$

Throughout the porous electrode, the following initial conditions in Equations 24 through 27 apply, where $c_{l,0} = 1000\ mol\ \text{m}^{-3}$ is the concentration of the stock electrolyte (1M) and $c_{s,0}$ [$mol\ \text{m}^{-3}$] is the initial concentration of lithium in the solid particles, which is calculated in Supplementary Table 3. The equilibrium potential, E_{eq} [V], is a function of SOC. In the

separator region, the same liquid-phase initial conditions apply, but there are no variables for the solid-phase.

$$\phi_l = \phi_{l,0} = 0 \tag{24}$$

$$\phi_s = \phi_{s,0} = E_{\text{eq}}(\text{SOC}) \tag{25}$$

$$c_l = c_{l,0} \tag{26}$$

$$c_s = c_{s,0} \tag{27}$$

3.2. 1D Battery Model

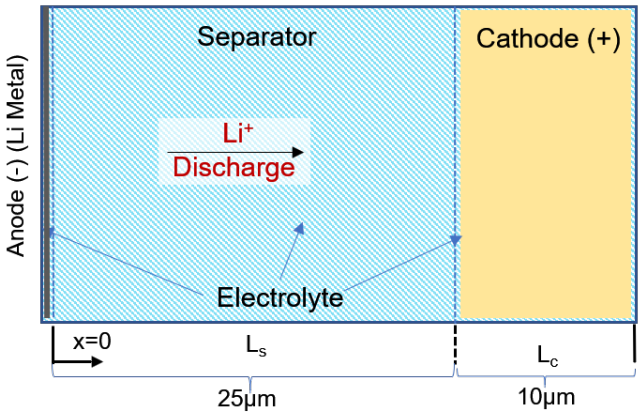

Supplementary Figure 21. Schematic of $LiFePO_4$|Li half-cell model with 1-D coordination shown.

A 1D model on the basis of the pseudo two-dimensional model was implemented to simulate the discharge of the $LiFePO_4$|Li cells by using COMSOL Multiphysics® under an isothermal scenario.[4-8] The geometry setup for the $LiFePO_4$|Li is shown in Supplementary Fig. 21, the cell contains a $LiFePO_4$ cathode, separator, electrolyte and a Lithium-metal anode. On the right, there is a porous $LiFePO_4$ electrode that is $10\mu m$ in thickness along the x-axis. On the left, there is a porous separator that is $25\ \mu m$ in thickness along the x-axis. The electrolyte material (LiTFSI in DOL/DME 1:1) is present throughout both of these domains, since both of the materials are porous. The left node on the edge of the geometry is modeled as an electrode surface to represent the surface of the pure lithium metal disk, which is modeled with a constant

current density to represent a constant C-rate from the current collector while discharging the half cell. The right node at the current collector surface has a no flux boundary condition, since lithium does not transfer into the current collector.

This 1D model is sufficient for relating electrode properties and parameters to the electrochemical performance of the cell. The simulated electrochemical performance was compared to the measured specific capacity (mAh g^{-1}) vs. voltage (V) curves obtained for charging between $V_{\min}$ [V] and $V_{\max}$ [V] at the constant C-rates of 1C, 10C, 20C, and 50C.

3.3. Constant Parameters

The parameters used in the $LiFePO_4$ half-cell COMSOL simulation are shown in Supplementary Table 3. The negative electrode refers to pure lithium metal, while the positive electrode refers to $LiFePO_4$. A formula is used for the value of the 1C discharge current, i_{1C} [A m^{-2}], so that when the thickness of the electrode, h_{pos} [m], particle density of active material particles in the positive electrode, ρ_{LFP} [kg m^{-3}], theoretical capacity in the electrode, $\tilde{Q}_{\text{theretical}}$ [C kg^{-1}], and/or electrolyte volume fraction, ε_l, are changed, which are taken from known experimental values, then the value of i_{1C} [A m^{-2}] is automatically calculated. The electrolyte conductivity, σ_l [S m^{-1}], transport number, $t_{\text{Li+}}$, thickness of the negative electrode, h_{neg} [m], thickness of the separator, h_{sep} [m], the minimum voltage, $V_{\min}$ [V], the maximum voltage, $V_{\max}$ [V], the initial lithium ion concentration in the electrolyte, $C_{l,0}$ [mol m^{-3}], and the C-rates, C [h^{-1}], are also all taken from experimental values. The electrolyte conductivity, σ_l [$S\ m^{-1}$], and transport number, $t_{\text{Li+}}$, are manipulated between the cases with and without MEM.

The values of the electrical conductivity in the positive electrode, σ_s [S m^{-1}], solid-phase diffusivity, D_s [m^2 s^{-1}], electrolyte diffusivity, D_l [m^2 s^{-1}], max solid lithium concentration in the positive electrode, $C_{s,\max}$ [mol m^{-3}], reference concentration, C_{ref} [mol m^{-3}], filler volume fraction in the positive electrode, ε_f, reaction rate constant for the positive electrode, k_{pos} [m s^{-1}], anodic transfer coefficient, α_{a}, cathodic transfer coefficient, α_{c}, active material particle radius, r_p [m], and Bruggeman coefficient, β, are all taken from values in the literature.

The values of the initial solid lithium concentration in the active material particles of the positive electrode, $C_{s,0}$ [mol m^{-1}], the reaction rate coefficient for the negative electrode, k_{neg} [m s^{-1}], the separator porosity, $\varepsilon_{l,\mathrm{sep}}$, and the temperature, T [K], are assumed. The separator porosity is chosen from typical industry values. The negative reaction rate constant is chosen to simulate the fast kinetics of the pure lithium-metal anode. A value of $T = 298$ K is used for the temperature, since the cells are cycled at room temperature. The model is assumed to be isothermal.

Supplementary Table 3. Constant parameters used in the $LiFePO_4$ half-cell COMSOL simulation.

Parameter	Equation/Value	Description	Source
i_{1C}	$h_{\mathrm{pos}}\rho_{LFP}\varepsilon_s\tilde{Q}_{\mathrm{theretical}} = 10\cdot10^{-6}\ \mathrm{m}\times 3{,}600{,}000\frac{\mathrm{g}}{\mathrm{m^3}}\times 0.56\times 0.150\frac{\mathrm{Ah}}{\mathrm{g}}\times 1\ \mathrm{h^{-1}} = 3\ \mathrm{A\ m^{-2}}$	1C discharge current	Calculated
C	1C, 10C, 20C, 50C	C rates	Experimental
h_{neg}	0	Thickness of negative electrode	Experimental
h_{sep}	$25\cdot10^{-6}$ m	Thickness of separator	Experimental
h_{pos}	$10\cdot10^{-6}$ m	Thickness of positive electrode	Experimental
h_{total}	$h_{\mathrm{neg}} + h_{\mathrm{sep}} + h_{\mathrm{pos}}$	Thickness of single stack	Calculated
ε_l	0.3	Electrolyte volume fraction in positive electrode	Measured
ε_f	0.14	Filler volume fraction in positive electrode	Assumed
ε_s	$1-\varepsilon_l-\varepsilon_f$	Active material volume fraction in positive electrode	Calculated
$\varepsilon_{l,\mathrm{sep}}$	0.4	Electrolyte volume fraction in separator	Assumed
$C_{l,0}$	1000 mol m^{-3}	Initial electrolyte salt concentration	Experimental
$C_{s,0}$	1000 mol m^{-3}	Initial concentration of solid lithium in positive electrode active material	Assumed

$C_{s,\max}$	21190 mol m^{-3}	Max concentration of solid lithium in positive electrode active material	[8]
C_{ref}	1000 mol m^{-3}	Reference concentration	[8]
$t_{\text{Li+}}$	0.29 (without MEM), 0.76 (with MEM)	Li-ion transference number in electrolyte	Experimental
σ_l	0.32 S/m (without MEM), 0.68 S/m (with MEM)	Li-ion conductivity in electrolyte	Experimental
σ_s	100 S m^{-1}	Electrical conductivity in positive electrode	[4]
D_s	$3.2 \cdot 10^{-13}$ m^2 s^{-1}	Solid-phase lithium diffusivity	[8]
r_p	$0.6 \cdot 10^{-6}$ m	Particle radius of positive electrode active material	[8]
ρ_{LFP}	3.6 g cm^{-3}	Active material particle density in positive electrode	Experimental
$\tilde{Q}_{\text{theretical}}$	150 mAh/g $= 5.4 \cdot 10^5$ C kg^{-1}	Theoretical specific capacity of positive electrode	Experimental
k_{neg}	$1 \cdot 10^{-3}$ m s^{-1}	Reaction rate coefficient for negative electrode	Assumed
k_{pos}	$1.4 \cdot 10^{-12}$ m s^{-1}	Reaction rate coefficient for positive electrode	[8]
α_{a}	0.5	Anodic transfer coefficient	[5]
α_{c}	0.5	Cathodic transfer coefficient	[5]
$V_{\min}$	2.5 V	Minimum voltage	Experimental
$V_{\max}$	4.2 V	Maximum voltage	Experimental
β	3.3	Bruggeman coefficient	[8]
F	96485 C mol^{-1}	Faraday's constant	Known Constant
T	298 K	Temperature	Assumed

3.4. List of Assumptions

A list of the assumptions made in the COMSOL battery simulations is shown in Supplementary Table 4.

Supplementary Table 4. List of Assumptions in COMSOL battery simulations.

- 1D Battery Model (no deviation in y or z direction)
- Isothermal Model
- No SEI Film Resistance
- No Stress or Strain
- No Dissolving-Depositing Species
- No Double Layer Capacitance
- Bruggeman Effective Transport
- All transport equations described in Supplementary Information Section 3.1
- All constant parameters described in Supplementary Information Section 3.3

3.5. Simulation Results

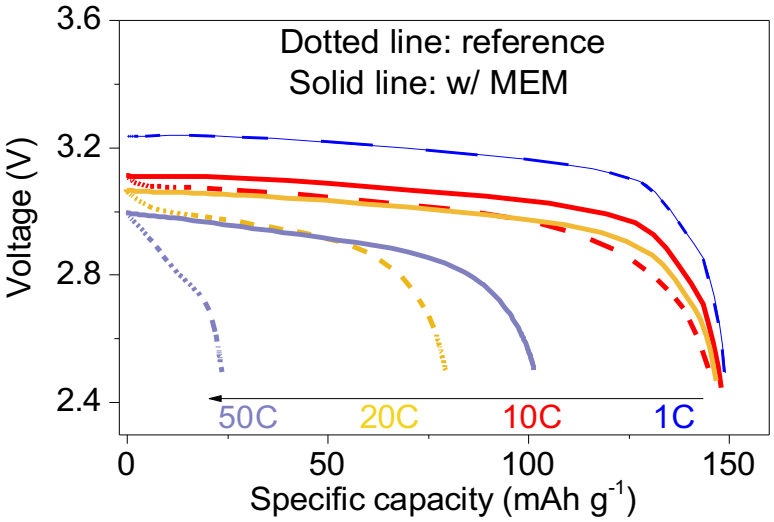

Supplementary Figure 22. Discharge profiles of conceptual $LiFePO_4$|Li cells at C rates of 1, 10, 20, and 50.

Supplementary Table 5. The simulated concentration gradient, electrolyte potential and discharge capacity at 10C, 20C and 50C of conceptual cell ($LiFePO_4$|Li) using electrolyte with and without MEM.

Discharge rate	Concentration at cathode side at discharge termination (mol m^{-3})		Potential drop (V)		Discharge duration (s)		Discharge capacity (mAh g^{-1})	
	reference	with MEM	reference	with MEM	reference	with MEM	reference	with MEM
10C	2	730	-0.25	-0.02	354	358	146	148
20C	0	408	-0.41	-0.04	96	178	79	147
50C	0	0	-0.43	-0.23	11	49	24	102

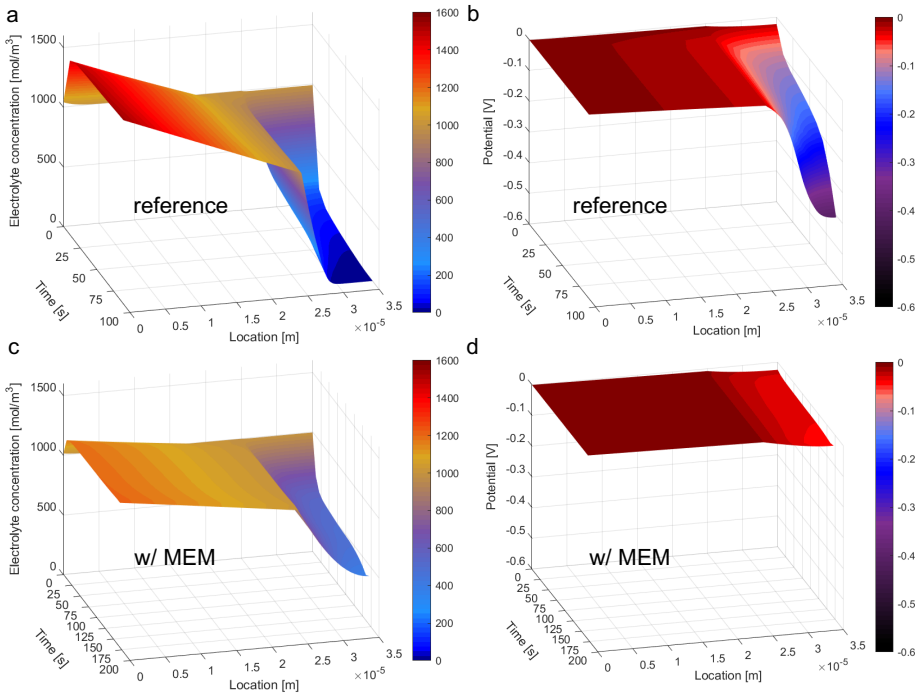

Supplementary Figure 23. (a, c) Concentration profiles and (b, d) electrolyte potential drops simulated from constant 20C discharging modeled $LiFePO_4$|Li cells. Note: (a-b) and (c-d) depict the cells using electrolyte parameters from LFS and LFS with 0.2 wt.% MEM, respectively.

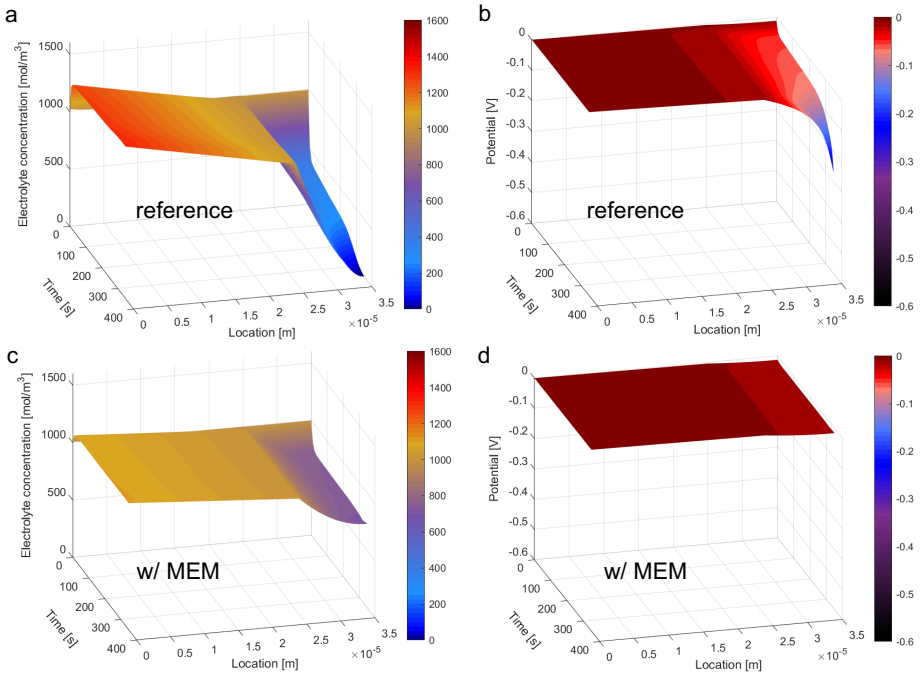

Supplementary Figure 24. (a, c) Concentration profiles and (b, d) electrolyte potential drops simulated from constant 10C discharging modeled $LiFePO_4$|Li cells. Note: (a-b) and (c-d) depict the cells using electrolyte parameters from LFS and LFS with 0.2 wt.% MEM, respectively.

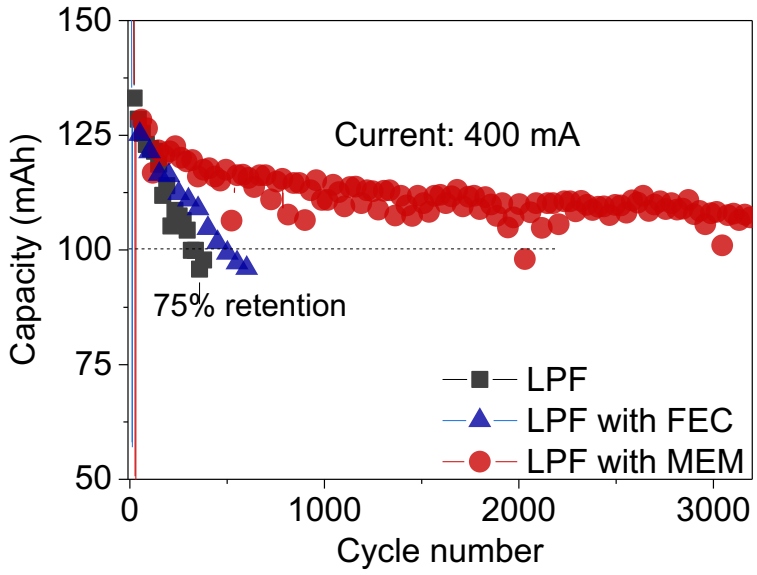

Supplementary Figure 25. Cycle comparison of pouch cells using LPF, LPF with FEC (fluoroethylene carbonate) and LPF with MEM.

Supplementary references

1. Ma J, Wong-Foy AG, Matzger AJ. The Role of Modulators in Controlling Layer Spacings in a Tritopic Linker Based Zirconium 2D Microporous Coordination Polymer. *Inorganic Chemistry* **54**, 4591-4593 (2015).

2. Ragon F*, et al.* Acid-functionalized UiO-66(Zr) MOFs and their evolution after intra-framework cross-linking: structural features and sorption properties. *Journal of Materials Chemistry A* **3**, 3294-3309 (2015).

3. Park C*, et al.* Molecular simulations of electrolyte structure and dynamics in lithium–sulfur battery solvents. *Journal of Power Sources* **373**, 70-78 (2018).

4. Northrop PWC, Ramadesigan V, De S, Subramanian VR. Coordinate Transformation, Orthogonal Collocation, Model Reformulation and Simulation of Electrochemical-Thermal Behavior of Lithium-Ion Battery Stacks. *Journal of The Electrochemical Society* **158**, A1461 (2011).

5. Danner T, Singh M, Hein S, Kaiser J, Hahn H, Latz A. Thick electrodes for Li-ion batteries: A model based analysis. *Journal of Power Sources* **334**, 191-201 (2016).

6. Cai L, White RE. Mathematical Modeling of a Lithium Ion Battery. In: *Proceedings of the COMSOL Conference* (2009).

7. Torchio M, Magni L, Gopaluni RB, Braatz RD, Raimondo DMJJoTES. Lionsimba: a matlab framework based on a finite volume model suitable for li-ion battery design, simulation, and control. **163**, A1192-A1205 (2016).

8. *Batteries & Fuel Cells Application Library Manual. COMSOL Application Gallery.* https://doc.comsol.com/5.3/doc/com.comsol.help.bfc/BatteriesAndFuelCellsApplicationLibraryManual.pdf (© 1998–2016 COMSOL).